

Unified theory of thermal transport in crystals and disordered solids

Michele Simoncelli¹, Nicola Marzari¹, and Francesco Mauri^{2*}

Crystals and glasses exhibit fundamentally different heat conduction mechanisms: the periodicity of crystals allows for the excitation of propagating vibrational waves that carry heat, as first discussed by Peierls¹; in glasses, the lack of periodicity breaks Peierls' picture and heat is mainly carried by the coupling of vibrational modes, often described by a harmonic theory introduced by Allen and Feldman². Anharmonicity or disorder are thus the limiting factors for thermal conductivity in crystals or glasses; hitherto, no transport equation has been able to account for both. Here, we derive such equation, resulting in a thermal conductivity that reduces to the Peierls and Allen-Feldman limits, respectively, in anharmonic-and-ordered or harmonic-and-disordered solids, while also covering the intermediate regimes where both effects are relevant. This approach also solves the long-standing problem of accurately predicting the thermal properties of crystals with ultralow or glass-like thermal conductivity^{3–10}, as we show with an application to a thermoelectric material representative of this class.

In 1929 Peierls¹ developed a semi-classical theory for heat conduction in terms of a Boltzmann transport equation (BTE) for propagating phonon wave packets. Nowadays, modern algorithms and computing systems allow to solve its linearized form (LBTE) either approximately (in the so-called single mode approximation (SMA)¹¹) or exactly, using iterative^{12,13}, variational¹⁴, or exact diagonalization^{15,16} methods; its accuracy has been highlighted in many studies^{14–17}. Nevertheless, these cases are characterized by having few, well-separated phonon branches and anharmonicity-limited thermal conductivity; we will refer to these in the following as “simple” crystals. In 1963 Hardy was able to express the thermal conductivity in terms of the phonon velocity operator¹⁸ and showed that its diagonal elements are the phonon group velocities entering the Peierls' BTE, while the off-diagonal terms, missing from it, are actually negligible in simple crystals¹⁸. In 1989 Allen and Feldman² envisioned that these off-diagonal elements, neglected so far, could become dominant in disordered regimes, where Peierls' picture breaks down due to the impossibility of defining phonons and group velocities. As a consequence, a harmonic theory of thermal transport in glasses was introduced, where disorder limits thermal conductivity and heat is carried by couplings of vibrational modes arising from the off-diagonal elements of the velocity operator (diffusons and locons^{19,20}). Recently, it has been argued that the diffuson conduction mechanism, typical of glasses, can also emerge in a third class of materials, termed “complex” crystals⁷, characterized by large unit cells and many quasi-degenerate phonon branches, where it coexists with phonon transport. Conversely, crystal-like prop-

agation mechanisms have been suggested also for glasses (propagons¹⁹) — albeit without a formal justification — in order to explain the experimental results¹⁹.

Here, we show that a more general theory exists, encompassing the emergence and coexistence of all these excitations, and reducing to the BTE in the semi-classical limit of a simple crystal, or to the Allen-Feldman formulation in the case of a harmonic glass.

We start by considering a crystal in the Born-Oppenheimer approximation, where we add perturbatively to a harmonic Hamiltonian²¹ H^{har} a collision term H^{col} accounting for anharmonicity²¹ and isotopic disorder²². Heat transfer is driven by a temperature gradient in real space (*i.e.* a space-dependent lattice vibrational energy) and in order to derive a more general transport equation we want to track excitations both in real and Fourier space. With this goal (see Methods for details) we introduce the bosonic operator $a(\mathbf{q})_{b\alpha}$ that annihilates vibrations with wave-vector \mathbf{q} for all atoms b in direction α (the Einstein summation convention is implied over repeated indexes)

$$a(\mathbf{q})_{b\alpha} = \frac{1}{\sqrt{2\hbar}} \left(\sqrt{D^{-1}(\mathbf{q})}_{b\alpha, b'\alpha'} P(\mathbf{q})_{b'\alpha'} - i \sqrt{D(\mathbf{q})}_{b\alpha, b'\alpha'} U^\dagger(\mathbf{q})_{b'\alpha'} \right). \quad (1)$$

Here $U(\mathbf{q})_{b\alpha} = \sqrt{M_b/N_c} \sum_{\mathbf{R}} u(\mathbf{R})_{b\alpha} e^{+i\mathbf{q}\cdot\mathbf{R}}$ and $P(\mathbf{q})_{b\alpha} = (\sqrt{M_b N_c})^{-1} \sum_{\mathbf{R}} p(\mathbf{R})_{b\alpha} e^{-i\mathbf{q}\cdot\mathbf{R}}$ are the Fourier representations of the displacement and momentum operators $u(\mathbf{R})_{b\alpha}$ and $p(\mathbf{R})_{b\alpha}$ of atom b in unit cell \mathbf{R} , with mass M_b and in a lattice containing N_c unit cells, and $D(\mathbf{q})$ is the dynamical matrix of the crystal with eigenvalues $\omega^2(\mathbf{q})_s$ (s labels the $3\cdot N_{\text{at}}$ phonon branches, N_{at} being the number of atoms in the unit cell). The usual commutation relations $[a(\mathbf{q})_{b\alpha}, a^\dagger(\mathbf{q}')_{b'\alpha'}] = \delta_{\mathbf{q}, \mathbf{q}'} \delta_{b, b'} \delta_{\alpha, \alpha'}$ are satisfied, and in terms of these operators H^{har} assumes the simple form:

$$H^{\text{har}} = \hbar \sum_{\mathbf{q}} \sqrt{D(\mathbf{q})}_{b\alpha, b'\alpha'} \left(a^\dagger(\mathbf{q})_{b\alpha} a(\mathbf{q})_{b'\alpha'} + \frac{1}{2} \delta_{b, b'} \delta_{\alpha, \alpha'} \right). \quad (2)$$

When a temperature gradient is imposed with couplings to external baths, the system's state — described by the density matrix ρ — undergoes an irreversible Markovian evolution described by the master equation²³

$$\frac{\partial \rho}{\partial t}(t) + \frac{i}{\hbar} [H^{\text{har}}, \rho(t)] = \left. \frac{\partial \rho(t)}{\partial t} \right|_{H^{\text{col}}}; \quad (3)$$

where the collision term $\left. \frac{\partial \rho(t)}{\partial t} \right|_{H^{\text{col}}}$ accounts for the transitions between the eigenstates of H^{har} driven by the perturbation H^{col} . Here we are interested in the vibrational energy, which is a one-body operator at the harmonic leading order. We can thus move to a formulation based on the one-body density matrix ρ_1 , which

¹Theory and Simulation of Materials (THEOS) and National Centre for Computational Design and Discovery of Novel Materials (MARVEL), École Polytechnique Fédérale de Lausanne, Lausanne, Switzerland. ²Dipartimento di Fisica, Università di Roma La Sapienza, Piazzale Aldo Moro 5, I-00185 Roma, Italy. *e-mail: francesco.mauri@uniroma1.it

is defined in terms of a trace over the Fock space²³: $\rho_1(\mathbf{q}, \mathbf{q}', t)_{b\alpha, b'\alpha'} = \text{Tr}(\rho(t) a^\dagger(\mathbf{q}')_{b'\alpha'} a(\mathbf{q})_{b\alpha})$. It follows from equation (3) that ρ_1 evolves according to:

$$\frac{\partial}{\partial t} \rho_1(\mathbf{q}, \mathbf{q}', t) + i \left(\sqrt{\mathbf{D}(\mathbf{q})} \rho_1(\mathbf{q}, \mathbf{q}', t) - \rho_1(\mathbf{q}, \mathbf{q}', t) \sqrt{\mathbf{D}(\mathbf{q}')} \right) = \frac{\partial}{\partial t} \rho_1(\mathbf{q}, \mathbf{q}', t) \Big|_{\text{Hcol}}. \quad (4)$$

For systems that are homogeneous in real space ρ_1 is diagonal: $\rho_1(\mathbf{q}, \mathbf{q}', t) = \rho_1(\mathbf{q}, \mathbf{q}, t) \delta_{\mathbf{q}, \mathbf{q}'}$; to study non-homogeneous systems it becomes useful to introduce the Wigner distribution \mathbf{W} , obtained by applying the Wigner-Weyl transformation to ρ_1 ²⁴:

$$W(\mathbf{R}, \mathbf{q}, t)_{b\alpha, b'\alpha'} = \sum_{\mathbf{q}''} \rho_1(\mathbf{q} + \mathbf{q}'', \mathbf{q} - \mathbf{q}'', t)_{b\alpha, b'\alpha'} e^{2i\mathbf{q}'' \cdot \mathbf{R}}. \quad (5)$$

It becomes apparent from equation (5) that a non-homogeneity in real space is related to a one-body density matrix with off-diagonal elements in reciprocal space. Now, we consider the out-of-equilibrium regime of a system perturbed by a small temperature gradient, appreciable over a length scale L much larger than the norms of the direct lattice vectors $|\mathbf{a}_i|$ ($i=1, 2, 3$). Applying the transformation (5) to equation (4), we can obtain the evolution for the Wigner distribution. Such evolution equation can be greatly simplified by using the hypothesis of having non-homogeneities only at mesoscopic scales or above, *i.e.* of having a one-body density matrix $\rho_1(\mathbf{q} + \mathbf{q}'', \mathbf{q} - \mathbf{q}'', t)$ that is sharply peaked and significantly different from zero only for $|\mathbf{q}''| \ll 2\pi|\mathbf{a}_i|^{-1}$. This allows us to perform a Taylor expansion for $\sqrt{\mathbf{D}(\mathbf{q} \pm \mathbf{q}'')}$ around $\mathbf{q}'' \rightarrow 0$, obtaining the simplified

equation:

$$\frac{\partial}{\partial t} \mathbf{W}(\mathbf{R}, \mathbf{q}, t) + i \left[\sqrt{\mathbf{D}(\mathbf{q})}, \mathbf{W}(\mathbf{R}, \mathbf{q}, t) \right] + \frac{1}{2} \left\{ \vec{\nabla}_{\mathbf{q}} \sqrt{\mathbf{D}(\mathbf{q})}, \cdot \vec{\nabla}_{\mathbf{R}} \mathbf{W}(\mathbf{R}, \mathbf{q}, t) \right\} = \frac{\partial}{\partial t} \mathbf{W}(\mathbf{R}, \mathbf{q}, t) \Big|_{\text{Hcol}}; \quad (6)$$

where the gradients appearing in the anticommutator are contracted using the scalar product. The spatial gradient $\vec{\nabla}_{\mathbf{R}}$ acts on the variable \mathbf{R} appearing in the exponential $e^{2i\mathbf{q}'' \cdot \mathbf{R}}$, whose characteristic length scale is $L \sim |\mathbf{q}''|^{-1} \gg |\mathbf{a}_i|$. Over such mesoscopic scale L the discrete variable \mathbf{R} can be considered as continuous and the gradient $\vec{\nabla}_{\mathbf{R}}$ well-defined. At this point, thanks to the locality in \mathbf{q} of equation (6), we can recast it in the phonon representation by applying the unitary transformation that diagonalizes $\mathbf{D}(\mathbf{q})$: $\mathcal{E}^*(\mathbf{q})_{s, b\alpha} \mathbf{D}(\mathbf{q})_{b\alpha, b'\alpha'} \mathcal{E}(\mathbf{q})_{s', b'\alpha'} = \omega^2(\mathbf{q})_s \delta_{s, s'}$. We thus introduce the following quantities

$$N(\mathbf{R}, \mathbf{q}, t)_{s, s'} = \mathcal{E}^*(\mathbf{q})_{s, b\alpha} W(\mathbf{R}, \mathbf{q}, t)_{b\alpha, b'\alpha'} \mathcal{E}(\mathbf{q})_{s', b'\alpha'}, \quad (7)$$

$$V^\beta(\mathbf{q})_{s, s'} = \mathcal{E}^*(\mathbf{q})_{s, b\alpha} \nabla_{\mathbf{q}}^\beta \sqrt{\mathbf{D}(\mathbf{q})}_{b\alpha, b'\alpha'} \mathcal{E}(\mathbf{q})_{s', b'\alpha'} \quad (8)$$

where the atomic and Cartesian indexes are replaced by the phonon branch index s . We define the diagonal matrix $\Omega(\mathbf{q})_{s, s'} = \omega(\mathbf{q})_s \delta_{s, s'}$ and denote with $\frac{\partial N(\mathbf{R}, \mathbf{q}, t)_{s, s'}}{\partial t} \Big|_{\text{Hcol}}$ the collision operator in the basis of the phonon modes. Equations (7) and (8) yield respectively a generalization of the phonon distributions and group velocities appearing in the BTE^{1,14}; in the absence of degeneracies (*i.e.* for $\omega(\mathbf{q})_s \neq \omega(\mathbf{q})_{s'} \forall s \neq s'$) the diagonal elements $s=s'$ of equation (7) and of equation (8) coincide, respectively, with the phonon distributions appearing in Peierls' equation and with their group velocities. Equation (6) in the phonon representation reads

$$\frac{\partial}{\partial t} \mathbf{N}(\mathbf{R}, \mathbf{q}, t) + i \left[\Omega(\mathbf{q}), \mathbf{N}(\mathbf{R}, \mathbf{q}, t) \right] + \frac{1}{2} \left\{ \vec{\mathbf{V}}(\mathbf{q}), \cdot \vec{\nabla}_{\mathbf{R}} \mathbf{N}(\mathbf{R}, \mathbf{q}, t) \right\} = \frac{\partial}{\partial t} \mathbf{N}(\mathbf{R}, \mathbf{q}, t) \Big|_{\text{Hcol}}. \quad (9)$$

This equation is the first main result of this paper, and offers a more general phonon transport equation, where phonon wave packets are not only allowed to propagate particle-like in space but also to tunnel, wave-like, from one branch to another. We note that the left-hand side of equation (9) does not contain \hbar , and it does not distinguish between fermions or bosons. Quantum statistics is instead enforced by the collision term at the right-hand side (see *e.g.* equation (11) later). The vibrational energy density can now be determined from the solution of equation (9): $E(\mathbf{R}, t) = \frac{\hbar}{\mathcal{V}N_c} \sum_{\mathbf{q}, s} (\mathbf{N}(\mathbf{R}, \mathbf{q}, t) \Omega(\mathbf{q}))_{s, s}$. Computing the time derivative of $E(\mathbf{R}, t)$ and using equation (9), one obtains the harmonic heat flux $\mathbf{J}(\mathbf{R}, t)$:

$$\mathbf{J}(\mathbf{R}, t) = \frac{1}{2} \frac{1}{\mathcal{V}N_c} \sum_{\mathbf{q}, s} \left(\vec{\mathbf{V}}(\mathbf{q}), \mathbf{N}(\mathbf{R}, \mathbf{q}, t) \right) \hbar \Omega(\mathbf{q})_{s, s}. \quad (10)$$

To compute the thermal conductivity we focus on the steady-state regime and search for a solution of equation (9)

linear in the temperature gradient. The right-hand side collision term can be written in a closed form approximation expressing the many-body collision operator (3) in terms of one-body quantities and linearizing it around the equilibrium temperature T ²³⁻²⁵

$$\frac{\partial}{\partial t} \mathbf{N}(\mathbf{R}, \mathbf{q}, t)_{s, s'} \Big|_{\text{Hcol}} = -(1 - \delta_{s, s'}) \frac{\Gamma(\mathbf{q})_s + \Gamma(\mathbf{q})_{s'}}{2} \mathbf{N}(\mathbf{R}, \mathbf{q}, t)_{s, s'} - \frac{\delta_{s, s'}}{\mathcal{V}N_c} \sum_{s'' \mathbf{q}''} A^T(\mathbf{q}, \mathbf{q}'')_{s, s''} (\mathbf{N}(\mathbf{R}, \mathbf{q}'', t)_{s'', s''} - \bar{N}^T(\mathbf{q}'')_{s''}); \quad (11)$$

where \mathcal{V} is the unit cell volume, $\bar{N}^T(\mathbf{q})_s = (\exp[\frac{\hbar\omega(\mathbf{q})_s}{k_B T}] - 1)^{-1}$ is the equilibrium Bose-Einstein distribution, $\Gamma(\mathbf{q})_s = (\mathcal{V}N_c)^{-1} A^T(\mathbf{q}, \mathbf{q})_{s, s} \delta_{s''}$ is the phonon linewidth and $A^T(\mathbf{q}, \mathbf{q}'')_{s, s''}$ is the standard collision operator that accounts for anharmonicity and isotopic disorder (for the third-order anharmonicities considered here, see equation (13) of Ref.¹⁴). Under these conditions, equation (9)

can be decoupled in its diagonal and off-diagonal parts, as shown in Methods; these two equations describe the evolution of the populations and coherences, respectively, using the standard nomenclature in this field. The equation for the populations turns out to be the standard Peierls' LBTE that can be solved exactly¹²⁻¹⁶; the equation for the coherences can be solved straightforwardly (see Methods).

$$\kappa^{\alpha\beta} = \kappa_{\text{P}}^{\alpha\beta} + \frac{\hbar^2}{k_{\text{B}}T^2} \frac{1}{\mathcal{V}N_{\text{c}}} \sum_{\mathbf{q}} \sum_{s \neq s'} \frac{\omega(\mathbf{q})_s + \omega(\mathbf{q})_{s'}}{2} V^{\alpha}(\mathbf{q})_{s,s'} V^{\beta}(\mathbf{q})_{s',s} \times \frac{\omega(\mathbf{q})_s \bar{N}^T(\mathbf{q})_s [\bar{N}^T(\mathbf{q})_s + 1] + \omega(\mathbf{q})_{s'} \bar{N}^T(\mathbf{q})_{s'} [\bar{N}^T(\mathbf{q})_{s'} + 1]}{4[\omega(\mathbf{q})_{s'} - \omega(\mathbf{q})_s]^2 + [\Gamma(\mathbf{q})_s + \Gamma(\mathbf{q})_{s'}]^2} [\Gamma(\mathbf{q})_s + \Gamma(\mathbf{q})_{s'}]; \quad (12)$$

where $\kappa_{\text{P}}^{\alpha\beta}$ is the standard Peierls contribution to the conductivity and the additional tensor, which we name $\kappa_{\text{C}}^{\alpha\beta}$, derives from the coherences' equation. The relevance of equation (12) is its capability to account for heat transfer associated to both the diagonal (populations) and off-diagonal (coherences) Wigner distribution elements. The former is associated to the particle-like propagation of phonon wave packets discussed by Peierls' semiclassical picture; the latter is related to the wave-like tunneling and loss of coherence between different vibrational eigenstates. Equation (12) highlights the conditions under which $\kappa_{\text{C}}^{\alpha\beta}$ is relevant, namely when the difference between the phonon frequencies is of the same order of the average phonon linewidth and, at the same time, the velocity operator has non-negligible off-diagonal elements — we will show later that this is what precisely happens in complex crystals. In simple crystals, instead, the present approach and the standard LBTE provide very similar results since, as we will show later, $\kappa_{\text{P}}^{\alpha\beta} \gg \kappa_{\text{C}}^{\alpha\beta}$. Since the thermal conductivity (12) derives from an exact linear-order solution of equation (9), it remains valid also in the hydrodynamic regime¹⁷. In the kinetic regime¹⁷ instead, a good estimation of $\kappa_{\text{P}}^{\alpha\beta}$ can be obtained using the SMA approximation, *i.e.* neglecting the scattering events that repopulate the diagonal $N(\mathbf{R}, \mathbf{q}, t)_{s,s}$. In practice, the SMA consists in replacing the collision matrix for the populations of equation (11) with its diagonal elements only: $A^T(\mathbf{q}, \mathbf{q}'')_{s,s''} \simeq (\mathcal{V}N_{\text{c}})\Gamma(\mathbf{q})_s \delta_{\mathbf{q},\mathbf{q}''} \delta_{s,s''}$. The equation for the coherences is unaffected by this approximation²⁵; it follows that the total SMA conductivity is given by an expression equal to the last term of equation (12), but with the summation running in full over s and s' (equation (26) in Methods). Last, we show in Methods how in the limit of a harmonic crystal with an infinitely large unit cell (*i.e.* with the Brillouin zone reduced to the Γ -point) the normalized trace of the coherences' conductivity tensor $\frac{1}{3}\kappa_{\text{C}}^{\alpha\alpha}$ reduces to the Allen-Feldman expression for glasses².

The perovskite CsPbBr₃, which belongs to a family of materials promising for thermoelectric energy conversion^{5,6}, is a good case study for this more general framework, as it features many quasi-degenerate phonon branches and its thermal properties^{5,6} are not correctly de-

scribed by the LBTE⁶. We compute from first-principles the harmonic Hamiltonian and the collision operator (see details in Methods), calculating the complete thermal conductivity of equation (12) as a function of temperature. The results are shown in figure (1) (we show here the SMA for κ^{xx} ; this is almost identical to the full solution (see Methods)): at 300 K the populations term contributes just 30% of the total conductivity, while the coherences term provides an additional 70%, leading to much closer agreement with experiments⁵ that becomes even more relevant in the high-temperature asymptotics. Conversely, at low temperature Peierls' term becomes dominant (at 50 K it provides 78% of the total conductivity). It can be seen that in the high temperature limit $\kappa_{\text{P}}^{\alpha\beta} \propto T^{-1}$, as predicted by Peierls' theory^{3,4,9,21}; this in broad disagreement with experiments. Instead, the present theory predicts a decay of κ^{xx} much milder than T^{-1} as shown here for CsPbBr₃, and as also present in many other complex crystals^{4,7-10,26}. We note in passing that the $\kappa_{\text{P}}^{\alpha\beta}$ calculated here and the one presented in Ref.⁶ are very

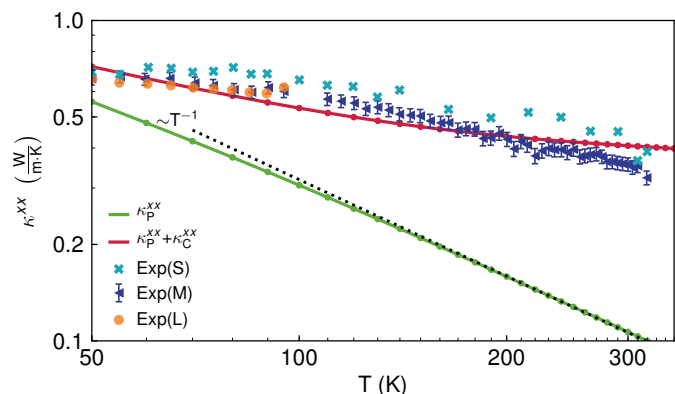


Figure 1. Bulk thermal conductivity of CsPbBr₃ as a function of temperature. “Exp(L)”, “Exp(M)” and “Exp(S)” refer to experiments⁵ on nanowires having respectively sections of 800×380 nm², 320×390 nm² and 300×160 nm²: their broad agreement supports the hypothesis of negligible finite-size boundary scattering⁵. Green, Peierls' LBTE conductivity, with its universal T^{-1} asymptotics (dotted line)^{3,4,9,21}. Red, conductivity from equation (12).

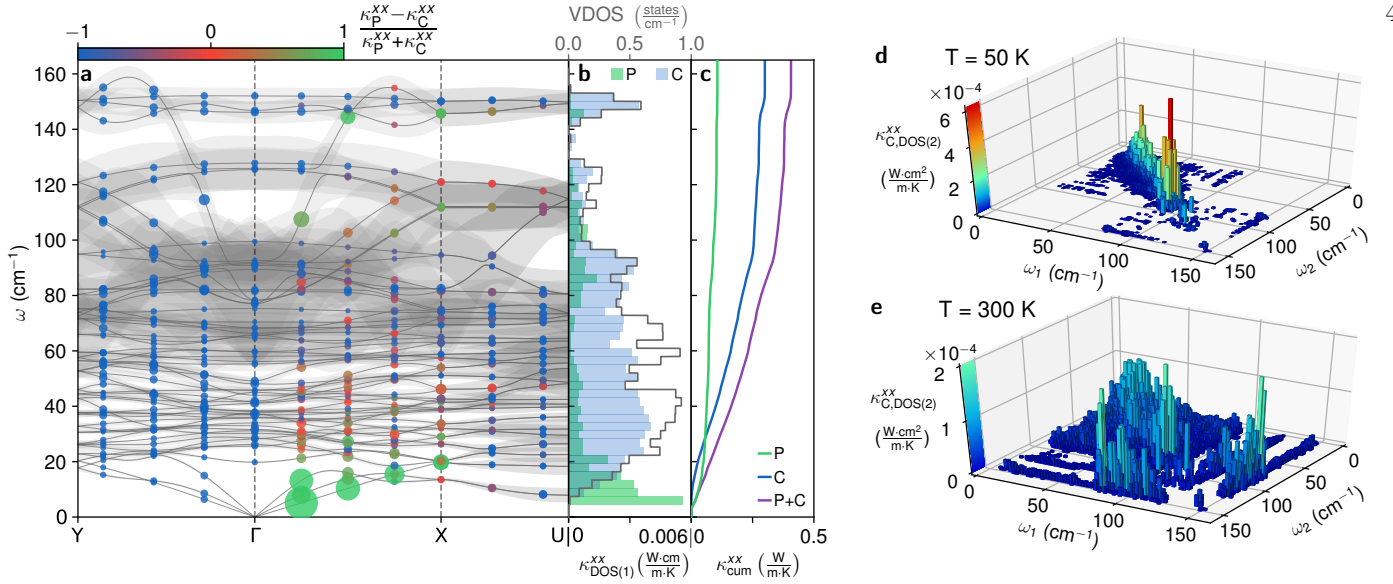


Figure 2. Vibrational properties and heat conduction mechanisms in CsPbBr₃. **a**, The phonon spectrum of CsPbBr₃ (gray lines) features low-energy flat branches, typical of rattling vibrations^{4,6,8}. The shaded gray areas are half the phonon linewidths ($\Gamma(\mathbf{q})_s/2$ for graphical clarity) at 300 K. Colored circles in the plot represent the phonon eigenstates (\mathbf{q}, s) sampled in the calculation; the area of each circle is related to its contribution to κ^{xx} at 300 K and the color identifies the origin of the contribution: green for populations' propagation and blue for coherences' anharmonic couplings (red corresponds to 50% of each). In the coherences' couplings between two modes (\mathbf{q}, s) and (\mathbf{q}, s') the contribution of the single mode s is determined as $C(\mathbf{q})_s/[C(\mathbf{q})_s+C(\mathbf{q})_{s'}]$, where $C(\mathbf{q})_s=\hbar^2/(k_B T^2)\omega^2(\mathbf{q})_s \bar{N}^T(\mathbf{q})_s[\bar{N}^T(\mathbf{q})_{s+1}]$ is the specific heat of a given phonon. **b**, Thermal conductivity density of states $\kappa_{\text{DOS}(1)}^{xx}$ of populations ("P", green) and coherences ("C", blue). The gray line shows the vibrational density of states (VDOS). **c**, Cumulative thermal conductivity (in purple) as a sum of the populations' contribution ("P") in green and coherences' one ("C") in blue. **d, e**, 2-dimensional density of states $\kappa_{\text{C,DOS}(2)}^{xx}$ for the contribution to the thermal conductivity of the coherences term at 50 K (**d**) and 300 K (**e**). The points on the diagonal $\omega_1=\omega_2$ correspond to degenerate eigenstates; the Allen-Feldman framework considers couplings only between these.

similar, confirming that all computational parameters are correctly accounted for. Figure (2a-c) shows that phonon branches with large group velocities and low anharmonicity provide a large contribution to the populations term; conversely, highly anharmonic flat bands contribute to the coherences term. The populations contribution originates mainly from low-frequency modes, while all the spectrum contributes to the coherences term. At 50 K, the 2-dimensional density of states for the coherences' thermal conductivity ($\kappa_{\text{C,DOS}(2)}^{xx}$, figure (2d)) shows couplings between quasi-degenerate states similarly to the case of harmonic glasses ($\Gamma(\mathbf{q})_s \rightarrow 0$). At 300 K (figure (2e)) $\kappa_{\text{C,DOS}(2)}^{xx}$ instead includes couplings between phonon modes having very different frequencies, driven by the large anharmonicity — therefore the corresponding heat conduction mechanism is intrinsically different from the one of harmonic glasses. In order to verify that the present theory reduces to the Peierls regime in the limit of simple crystals, we computed the room-temperature (300 K) thermal conductivity (12) of silicon and diamond. We found that for these crystals the coherences term is negligible: for silicon $\kappa_{\text{P}}^{xx}=142.83$ W/(m·K) vs. $\kappa_{\text{C}}^{xx}=0.23$ W/(m·K); for diamond $\kappa_{\text{P}}^{xx}=2780.07$ W/(m·K) vs. $\kappa_{\text{C}}^{xx}=0.03$ W/(m·K).

In summary, we have derived from the Wigner phase space formulation of quantum mechanics a general transport equation (9) able to account rigorously and simultaneously for anharmonicity and disorder, leading to a thermal conductivity (12) that adds an interbranch tunneling term for the coherences; this equation (12) reduces to the Peierls' BTE in the limit of simple crystals, and it provides a rigorous derivation of the BTE for phonon populations

first heuristically derived by Peierls¹. Also, in the limit of harmonic glasses, the thermal conductivity (12) reduces to the Allen-Feldman limit; equation (12) is more general and encompasses all intermediate cases, applying also to anharmonic glasses. The LBTE approach, which accounts for populations only, greatly underestimates the thermal conductivity of complex crystals^{4,6,7,9,10} that ubiquitously display a glass-like high-temperature behavior (*i.e.* decay milder than the universal T^{-1} trend predicted by Peierls' theory^{3,4,9,21}) and that up to now has been only heuristically explained by several models^{7,26-28}. In the present approach, the correct conductivity is recovered, and its high-temperature decay (figure (1)).

We note in passing that a complementary approach to these transport equations is to compute the thermal conductivity via the Green-Kubo method^{20,29-32}, which is based on molecular dynamics and is exact, although computationally more expensive, provided one is in the classical Maxwell-Boltzmann high-temperature limit (*i.e.* at $T \gg T_D$, where T_D is the Debye temperature). Coherences' effects have been thoroughly studied in the context of electronic transport^{23,24,33} and it is worth mentioning that the term $\kappa_{\text{C}}^{\alpha\beta}$ has some analogies with the electronic current related to the Zener interband transitions³³. However, thermal transport is fundamentally different from electronic transport since the full phonon spectrum contributes to the heat flow, while for electrons the current originates only from the bands close to the Fermi level. This novel formulation is also going to be relevant to applied research, as it allows to predict the low thermal conductivity of target materials for thermoelectric energy conversion^{6,8}.

Acknowledgements

Author contributions

The project was conceived by all authors. M.S. performed the numerical calculations and prepared the figures with inputs from N.M and F.M. All authors contributed to the redaction of the manuscript.

Competing interests

The authors declare no competing interests.

Additional information

Correspondence and request of materials should be addressed to F.M.

Methods

Bosonic operators in the Cartesian basis. In order to describe heat transfer driven by a temperature gradient (*i.e.* a spatially-dependent lattice vibrational energy), we need to keep track of the vibrations' location in real space. This is possible using the Fourier transform of the bosonic operator defined in equation (1):

$$\begin{aligned} a(\mathbf{R})_{b\alpha} &= \frac{1}{\sqrt{N_c}} \sum_{\mathbf{q}} a(\mathbf{q})_{b\alpha} e^{+i\mathbf{q}\cdot\mathbf{R}} = \\ &= \frac{1}{\sqrt{2\hbar}} \sum_{\mathbf{R}''} \left(\sqrt[4]{G^{-1}}_{\mathbf{R}b\alpha, (\mathbf{R}+\mathbf{R}'')b'\alpha'} \frac{p(\mathbf{R}+\mathbf{R}'')_{b'\alpha'}}{\sqrt{M_{b'}}} \right. \\ &\quad \left. - i\sqrt{M_{b'}} u(\mathbf{R}+\mathbf{R}'')_{b'\alpha'} \sqrt[4]{G}_{(\mathbf{R}+\mathbf{R}'')b'\alpha', \mathbf{R}b\alpha} \right); \end{aligned} \quad (13)$$

since, as we will show now, it is related to vibrations localized around the lattice site indexed by (\mathbf{R}, b, α) . The tensor $G_{\mathbf{R}b\alpha, (\mathbf{R}+\mathbf{R}'')b'\alpha'}$ appearing in equation (13) is related to the interatomic harmonic force constants in real space²¹, $\Phi_{\mathbf{R}b\alpha, (\mathbf{R}+\mathbf{R}'')b'\alpha'}$:

$$G_{\mathbf{R}b\alpha, (\mathbf{R}+\mathbf{R}'')b'\alpha'} = \frac{\Phi_{\mathbf{R}b\alpha, (\mathbf{R}+\mathbf{R}'')b'\alpha'}}{\sqrt{M_b M_{b'}}}; \quad (14)$$

it is translation-invariant and decays to zero for $\mathbf{R}'' \rightarrow \infty$ ^{21,34}. The harmonic Hamiltonian (2) can be written in terms of the vibrational energy field $H^{\text{har}} = \sum_{\mathbf{R}, b, \alpha} \mathcal{H}(\mathbf{R})_{b\alpha}$,

where

$$\begin{aligned} \mathcal{H}(\mathbf{R})_{b\alpha} &= \frac{p^2(\mathbf{R})_{b\alpha}}{2M_b} + \\ &+ \frac{1}{2} \left(\sum_{\mathbf{R}'} \sqrt{G}_{\mathbf{R}b\alpha, (\mathbf{R}+\mathbf{R}')b'\alpha'} \sqrt{M_{b'}} u(\mathbf{R}+\mathbf{R}')_{b'\alpha'} \right) \times \\ &\times \left(\sum_{\mathbf{R}''} \sqrt{G}_{\mathbf{R}b\alpha, (\mathbf{R}+\mathbf{R}'')b'\alpha''} \sqrt{M_{b''}} u(\mathbf{R}+\mathbf{R}'')_{b'\alpha''} \right). \end{aligned} \quad (15)$$

In terms of the bosonic operators $a^\dagger(\mathbf{R})_{b\alpha}$, $a(\mathbf{R})_{b\alpha}$, the energy field (15) becomes:

$$\begin{aligned} \mathcal{H}(\mathbf{R})_{b\alpha} &= \hbar \sum_{\mathbf{R}', \mathbf{R}''} \sqrt[4]{G}_{\mathbf{R}b\alpha, (\mathbf{R}+\mathbf{R}')b'\alpha'} \sqrt[4]{G}_{\mathbf{R}b\alpha, (\mathbf{R}+\mathbf{R}'')b'\alpha''} \times \\ &\times \left(a^\dagger(\mathbf{R}+\mathbf{R}')_{b'\alpha'} a(\mathbf{R}+\mathbf{R}'')_{b'\alpha''} + \frac{1}{2} \delta_{\mathbf{R}', \mathbf{R}''} \delta_{b', b''} \delta_{\alpha', \alpha''} \right). \end{aligned} \quad (16)$$

From the decay to zero of $G_{\mathbf{R}b\alpha, (\mathbf{R}+\mathbf{R}'')b'\alpha'}$ for $\mathbf{R}'' \rightarrow \infty$, it follows that the excitation created by $a^\dagger(\mathbf{R})_{b\alpha}$ has an energy distribution $E(\mathbf{R}+\mathbf{R}'')_{\mathbf{R}b\alpha}$ localized around the position \mathbf{R} ³⁴:

$$\begin{aligned} E(\mathbf{R}+\mathbf{R}'')_{\mathbf{R}b\alpha} &= \sum_{b''\alpha''} \langle 0 | a(\mathbf{R})_{b\alpha} \mathcal{H}(\mathbf{R}+\mathbf{R}'')_{b''\alpha''} a^\dagger(\mathbf{R})_{b\alpha} | 0 \rangle \\ &\quad - \sum_{b''\alpha''} \langle 0 | \mathcal{H}(\mathbf{R}+\mathbf{R}'')_{b''\alpha''} | 0 \rangle \\ &= \hbar \sum_{b''\alpha''} \left(\sqrt[4]{G}_{\mathbf{R}''b''\alpha'', \mathbf{0}b\alpha} \right)^2, \end{aligned} \quad (17)$$

where we have used the translational invariance of the tensor \mathbf{G} to simplify the last equation: $\sqrt[4]{G}_{(\mathbf{R}+\mathbf{R}'')b''\alpha'', \mathbf{R}b\alpha} = \sqrt[4]{G}_{\mathbf{R}''b''\alpha'', \mathbf{0}b\alpha}$. We have therefore demonstrated that the operator (13) creates vibrations localized around the lattice position \mathbf{R} ; hence, performing the Fourier transform of the operator (1) it is possible to keep track of the vibrations' locations in real space. In contrast, the more common phonon-eigenmodes basis, obtained by the transformation (discussed in equations (7,8) of the main text):

$$a(\mathbf{q})_{s'} = \mathcal{E}^*(\mathbf{q})_{s', b'\alpha'} a(\mathbf{q})_{b'\alpha'}; \quad (18)$$

does not allow such a real space-based description. In fact, the operator $a(\mathbf{q})_{s'}$ does not have a direct correspondence with the location of vibrations in real space, due to the phase indeterminacy of the eigenstates $\mathcal{E}(\mathbf{q})_{s', b'\alpha'}$ of the dynamical matrix $\mathbf{D}(\mathbf{q})$. This becomes apparent considering the following gauge transformation, allowed by the phase freedom on $\mathcal{E}(\mathbf{q})_{s', b'\alpha'}$ at each \mathbf{q} -point:

$$\tilde{a}(\mathbf{q})_s = a(\mathbf{q})_s e^{i\mathbf{q}\cdot\mathbf{R}_\Delta}; \quad (19)$$

where \mathbf{R}_Δ is a direct lattice vector. Despite $\tilde{a}(\mathbf{q})_s$ and $a(\mathbf{q})_s$ being equivalent for a description in Fourier space, their real space representations are shifted by \mathbf{R}_Δ :

$$\begin{aligned} a(\mathbf{R})_s &= \frac{1}{\sqrt{N_c}} \sum_{\mathbf{q}} a(\mathbf{q})_s e^{+i\mathbf{q}\cdot\mathbf{R}}; \\ \tilde{a}(\mathbf{R})_s &= \frac{1}{\sqrt{N_c}} \sum_{\mathbf{q}} \tilde{a}(\mathbf{q})_s e^{+i\mathbf{q}\cdot\mathbf{R}} = a(\mathbf{R}+\mathbf{R}_\Delta)_s. \end{aligned} \quad (20)$$

It is worth mentioning that this mirrors the electronic case, where the phase indeterminacy of the Bloch orbitals is reflected in the non-uniqueness of the transformation into Wannier functions³⁵. In this work, the use of the Cartesian basis — which has no phase freedom — renders the real space description and hence the Wigner distribution (5) well-defined.

Decoupling of equation (9). We consider the steady-state regime, in which a small, slowly varying temperature gradient ∇T is established throughout the system. We look for a solution linear in the temperature gradient ∇T ¹⁴ on the distribution corresponding to the local equilibrium temperature³⁶ $T(\mathbf{x})$:

$$N(\mathbf{x}, \mathbf{q})_{s, s'} = \bar{N}^T(\mathbf{q})_s \delta_{s, s'} + \bar{n}^T(\mathbf{x}, \mathbf{q})_s \delta_{s, s'} + \bar{n}^{(1)}(\mathbf{q})_{s, s'} \cdot \nabla T(\mathbf{x}); \quad (21)$$

where $\bar{n}^T(\mathbf{x}, \mathbf{q})_s \delta_{s,s'}$ accounts for the local equilibrium temperature: $\bar{n}^T(\mathbf{x}, \mathbf{q})_s = \frac{d\bar{N}^T(\mathbf{q})_s}{dT}(T(\mathbf{x}) - T)$; the term $\bar{n}^{(1)}(\mathbf{q})_{s,s'} \cdot \nabla T(\mathbf{x})$ is, in general, non-diagonal in s, s' and contains the information concerning the deviation of the full solution from the local equilibrium solution — it is assumed to be of the order of the temperature gradient, as in previous work^{14,16}. Considering only the first-order term in ∇T , we obtain an equation that is decoupled in its diagonal and off-diagonal parts. The diagonal part turns out to be the usual LBTE for the populations¹⁴:

$$\begin{aligned} \vec{V}(\mathbf{q})_{s,s} \cdot \left(\frac{\partial N^T(\mathbf{q})_s}{\partial T} \nabla T(\mathbf{x}) \right) &= \\ &= -\frac{1}{\mathcal{V}N_c} \sum_{s'' \mathbf{q}''} A^T(\mathbf{q}, \mathbf{q}'')_{s,s''} (\bar{n}^{(1)}(\mathbf{q}'')_{s'',s''} \cdot \nabla T(\mathbf{x})); \end{aligned} \quad (22)$$

which can be solved approximately (in the SMA¹¹) or exactly¹²⁻¹⁶. The equation for the coherences ($s \neq s'$) is:

$$\begin{aligned} \frac{1}{2} \left(\frac{\partial N^T(\mathbf{q})_s}{\partial T} + \frac{\partial N^T(\mathbf{q})_{s'}}{\partial T} \right) \vec{V}(\mathbf{q})_{s,s'} \cdot \nabla T(\mathbf{x}) &= \\ - \left(i(\omega(\mathbf{q})_s - \omega(\mathbf{q})_{s'}) + \frac{\Gamma(\mathbf{q})_s + \Gamma(\mathbf{q})_{s'}}{2} \right) \bar{n}^{(1)}(\mathbf{q})_{s,s'} \cdot \nabla T(\mathbf{x}). \end{aligned} \quad (23)$$

Equation (23) can be solved exactly and straightforwardly,

$$\begin{aligned} \kappa_{\text{SMA}}^{\alpha\beta} &= \frac{\hbar^2}{k_B T^2} \frac{1}{\mathcal{V}N_c} \sum_{\mathbf{q}} \sum_{s,s'} \frac{\omega(\mathbf{q})_s + \omega(\mathbf{q})_{s'}}{2} V^\alpha(\mathbf{q})_{s,s'} V^\beta(\mathbf{q})_{s',s} \times \\ &\times \frac{\omega(\mathbf{q})_s \bar{N}^T(\mathbf{q})_s [\bar{N}^T(\mathbf{q})_s + 1] + \omega(\mathbf{q})_{s'} \bar{N}^T(\mathbf{q})_{s'} [\bar{N}^T(\mathbf{q})_{s'} + 1]}{4[\omega(\mathbf{q})_{s'} - \omega(\mathbf{q})_s]^2 + [\Gamma(\mathbf{q})_s + \Gamma(\mathbf{q})_{s'}]^2} [\Gamma(\mathbf{q})_s + \Gamma(\mathbf{q})_{s'}]; \end{aligned} \quad (26)$$

where we stress that the summation over s, s' in equation (26) includes the diagonal terms $s=s'$ (in contrast, these terms are excluded from the summation in equation (12)). We highlight how the coherences' conductivity $\kappa_C^{\alpha\beta}$ remains exact (*i.e.* as in equation (12)) also in the context of the SMA approximation. This can be understood from equation (11), where it is apparent that the coherences are affected only by scattering events that yield a decrease of the off-diagonal ($s \neq s'$) Wigner distribution²⁵ $N(\mathbf{R}, \mathbf{q}, t)_{s,s'}$ (depopulation). Therefore, when the scattering events that yield an increase of the populations are neglected in the SMA approximation, the coherence equation — affected by depopulation only — is left unchanged³⁴ and thus yields the same value for $\kappa_C^{\alpha\beta}$ reported in equation (12).

As a final remark for this section, it is worth mentioning that the equations for κ_P^{xx} in the work of Fugallo *et al.*¹⁴ are recovered by choosing the eigenstates of H^{har} in the degenerate subspaces to be eigenstates of $\mathbf{V}^x(\mathbf{q})$ and neglecting the term $\kappa_C^{\alpha\beta}$.

yielding ($s \neq s'$):

$$\begin{aligned} n^{(1),\alpha}(\mathbf{q})_{s,s'} &= -\frac{\hbar}{k_B T^2} V^\alpha(\mathbf{q})_{s,s'} \times \\ &\frac{\omega(\mathbf{q})_s \bar{N}^T(\mathbf{q})_s [\bar{N}^T(\mathbf{q})_s + 1] + \omega(\mathbf{q})_{s'} \bar{N}^T(\mathbf{q})_{s'} [\bar{N}^T(\mathbf{q})_{s'} + 1]}{2i[\omega(\mathbf{q})_s - \omega(\mathbf{q})_{s'}] + [\Gamma(\mathbf{q})_s + \Gamma(\mathbf{q})_{s'}]}. \end{aligned} \quad (24)$$

We stress that the simplicity of the equation for the coherences (23) implies that the computational cost for finding its solution is negligible compared to the one for solving exactly the populations' equation (22).

SMA approximation and properties of $\kappa^{\alpha\beta}$

In the kinetic regime¹⁷, a good estimate of the Peierls' conductivity $\kappa_P^{\alpha\beta}$ appearing in equation (12) is given by the SMA approximation, *i.e.* $\kappa_P^{\alpha\beta} \simeq \kappa_{\text{P,SMA}}^{\alpha\beta}$ where

$$\kappa_{\text{P,SMA}}^{\alpha\beta} = \frac{\hbar^2}{k_B T^2} \frac{1}{\mathcal{V}N_c} \sum_{\mathbf{q},s} \frac{\omega^2(\mathbf{q})_s \bar{N}^T(\mathbf{q})_s [\bar{N}^T(\mathbf{q})_s + 1]}{\Gamma(\mathbf{q})_s} V^\alpha(\mathbf{q})_{s,s} V^\beta(\mathbf{q})_{s,s}. \quad (25)$$

Within the SMA approximation, the total thermal conductivity $\kappa^{\alpha\beta}$ is approximated by $\kappa_{\text{SMA}}^{\alpha\beta} = \kappa_{\text{P,SMA}}^{\alpha\beta} + \kappa_C^{\alpha\beta}$, which can be written in the following compact form:

The limit of a harmonic crystal with infinite unit cell: Allen-Feldman equation. Here we show that in the limit of a harmonic crystal with an infinite unit cell (*i.e.* in the case of a harmonic glass, whose Brillouin zone is reduced to the Γ -point), the term $\kappa_C^{\alpha\beta}$ mathematically reduces to the Allen-Feldman expression for the thermal conductivity of harmonic glasses^{2,37}:

$$\kappa_A = \frac{1}{V_t} C_i(T) D_i(T); \quad (27)$$

where $i=1, \dots, 3 \cdot N_{\text{at}}^{\text{tot}}$ with $N_{\text{at}}^{\text{tot}}$ the total number of atoms in the (ideally infinite) single unit cell of the glass and V_t its (ideally infinite) volume. The mode specific heat $C_i(T)$ is:

$$C_i(T) = \left(\frac{\hbar \omega_i^2}{V_t T} \right) \left(-\frac{\partial \bar{N}_i}{\partial \omega_i} \right); \quad (28)$$

where $\bar{N}_i = (\exp[\hbar \omega_i / (k_B T)] - 1)^{-1}$ is the Bose-Einstein distribution and the mode diffusivity $D_i(T)$ is:

$$D_i(T) = \frac{\pi V_t^2}{3 \hbar^2 \omega_i^2} \frac{\hbar^2}{V^2} \sum_{j \neq i} \left| \vec{V}_{\text{AA}}(\mathbf{q})_{i,j} \frac{\omega_i + \omega_j}{2} \right|^2 \delta(\omega_i - \omega_j). \quad (29)$$

$V_{AA}^\beta(\mathbf{q})_{s,s'}$ is the velocity operator defined by Auerbach and Allen³⁸, which is related to the velocity operator (8) derived in this work:

$$V_{AA}^\beta(\mathbf{q})_{s,s'} = \frac{\omega(\mathbf{q})_s + \omega(\mathbf{q})_{s'}}{2\sqrt{\omega(\mathbf{q})_s\omega(\mathbf{q})_{s'}}} V^\beta(\mathbf{q})_{s,s'}. \quad (30)$$

The Dirac delta in equation (29) implies that these two velocity operators in equation (30) are equivalent in the computation of the Allen-Feldman diffusivities (29).

Equation (27) is derived under the hypothesis of extreme disorder — *i.e.* the phonon wave-packets do not propagate far enough to sample the periodicity of the medium, rendering it impossible to assign them a wave vector or a group velocity. In practice, this corresponds to neglecting the thermal conductivity contributions coming from the diagonal elements of the velocity operator (otherwise, at the harmonic order, these would yield a divergent thermal conductivity³⁹). Within such extreme disorder assumption, we are left with the coherences' term and we will show now that $\frac{1}{3}\kappa_C^\alpha$ is equivalent to the Allen-Feldman formula (27). Let us start by writing explicitly part of equation (28):

$$-\frac{\partial \bar{N}(\mathbf{q})_s}{\partial \omega(\mathbf{q})_s} \frac{\hbar \omega(\mathbf{q})_s}{V_t T} = \frac{1}{\mathcal{V} N_c} \frac{\hbar^2}{k_B T^2} \omega(\mathbf{q})_s \bar{N}(\mathbf{q})_s (\bar{N}(\mathbf{q})_s + 1); \quad (31)$$

where we have used $V_t = \mathcal{V} N_c$. Taking first the limit $\Gamma(\mathbf{q})_s \rightarrow \eta \forall (s, \mathbf{q})$ and then $\eta \rightarrow 0$, we have that the coherences' term in equation (12) becomes:

$$\begin{aligned} \kappa_{\text{dis}}^{\alpha\beta} = & - \sum_{\mathbf{q}, s \neq s'} \frac{\hbar \omega(\mathbf{q})_s^2}{V_t T} \frac{\partial \bar{N}(\mathbf{q})_s}{\partial \omega(\mathbf{q})_s} \frac{\pi}{\omega(\mathbf{q})_s} \delta(\omega(\mathbf{q})_{s'} - \omega(\mathbf{q})_s) \\ & \times \frac{\omega(\mathbf{q})_s + \omega(\mathbf{q})_{s'}}{2} V^\alpha(\mathbf{q})_{s,s'} V^\beta(\mathbf{q})_{s',s}; \end{aligned} \quad (32)$$

where we have obtained the delta function as the limit of a Lorentzian for $\Gamma(\mathbf{q})_s \rightarrow \eta \rightarrow 0$. It follows that, defining $\kappa_A = \kappa_{\text{dis}}^{\alpha\alpha}/3$ and in the case of a Brillouin zone reduced to the Γ -point, we recover the Allen-Feldman formula:

$$\kappa_A = \frac{1}{3} \sum_{s' \neq s} - \frac{\hbar \omega_s^2}{V_t T} \frac{\partial \bar{N}_s}{\partial \omega_s} \frac{\pi}{\omega_s^2} \delta(\omega_{s'} - \omega_s) \left(\frac{\omega_s + \omega_{s'}}{2} \right)^2 V_{s,s'}^\alpha V_{s',s}^\alpha; \quad (33)$$

where $\omega_s = \omega(\mathbf{q}=\mathbf{0})_s$, $\bar{N}_s = \bar{N}(\mathbf{q}=\mathbf{0})_s$ and $\vec{V} = \vec{V}(\mathbf{q}=\mathbf{0})$.

Phonon linewidths distribution. Figure (3) shows the distribution of the phonon linewidths for CsPbBr₃ at different temperatures. The distribution spans a range of about 4 orders of magnitude (from about 10^{-2} cm⁻¹ to about 10^2 cm⁻¹); consequently, couplings between vibrational eigenstates having very different frequencies are allowed, as shown in figure (2d,e). Increasing the temperature yields an increase of the phonon linewidths, with consequent higher $\kappa_C^{\alpha\beta}$ — since more couplings are allowed — and lower $\kappa_B^{\alpha\beta}$.

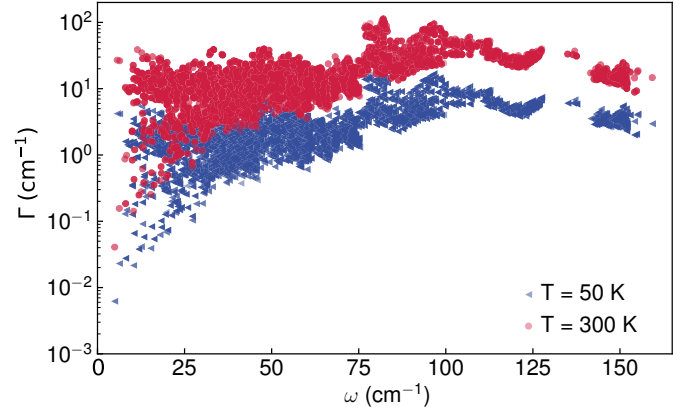


Figure 3. Phonon linewidths distribution of CsPbBr₃. The linewidths at 50 K and 300 K are respectively reported in blue and red. An increase in temperature results in a shift of the linewidths towards larger values.

Computational details. The experimental structure of orthorhombic CsPbBr₃⁴⁰ with *Pnma* space group (Crystallographic Open Database⁴¹ id: 4510745) is first converted into an equivalent structure with *Pbnm* space group using VESTA⁴², to allow a direct comparison with other references on this material^{5,43}. The first-principles equilibrium lattice parameters are then determined using Quantum ESPRESSO⁴⁴, the PBEsol exchange-correlation functional and GBRV⁴⁵ pseudopotentials. The PBEsol functional is selected on the basis of its good agreement between first-principles and experimental lattice parameters^{6,40} (see table (I)) and its capability to accurately describe the vibrational properties of inorganic halide perovskites⁶. Kinetic energy cutoffs of 50 and 400 Ry are used for the wave functions and the charge density. The Brillouin zone is integrated with a Monkhorst-Pack mesh of $5 \times 5 \times 4$ points, with a (1,1,1) shift. Second-order force constants are computed on a $4 \times 4 \times 4$ mesh using density-functional perturbation theory⁴⁶ as implemented in Quantum ESPRESSO. In order to obtain the third-order force constants using the PBEsol functional, the finite-difference method implemented in ShengBTE⁴⁷ is used, together with the interconversion software from ShengBTE to Quantum ESPRESSO available in the D3Q package⁴⁸. Third-order force constants are computed on a $2 \times 2 \times 2$ mesh and considering interactions up to the third-nearest neighbors. All the force constants are Fourier interpolated on $8 \times 7 \times 5$ grid for the thermal conductivity calculations. In the latter, natural-abundance isotopic scattering^{11,22} is considered in addition to third-order anharmonicity^{13,14,49-52}. From the force constants, the phonon frequencies and the full non-diagonal anharmonic scattering operator are computed as in previous work¹⁴. The anharmonic scattering operator is then modified to account for the coherences' term reported in equation (11). In figure (1), a smearing σ of 2 cm⁻¹ is used to compute the delta function appearing in the scattering operator. Results are converged with respect to the choice of this parameter: changing σ to 1 cm⁻¹ and 5 cm⁻¹ produces populations, coherences and total thermal conductivities with a maximum relative deviation of 2.6% from the data of figure (1). These latter refer to the single-mode

relaxation time approximation (SMA); the exact thermal conductivity is always compatible within 0.7% to its SMA value. Performing the thermal conductivity calculations using force constants that are Fourier interpolated on a $4 \times 4 \times 3$ mesh produces data compatible with the ones reported in figure (1), which use a $8 \times 7 \times 5$ mesh. In particular, the maximum relative deviation are respectively 1.8% for the populations in the SMA and 0.9% for the coherences' thermal conductivity. As anticipated in the main text, the data shown in figure (1) for $\kappa_P^{\alpha\beta}$ are compatible with the theoretical results presented in Ref.⁶ (and related Supplementary Material). In particular, the direction xx in this work corresponds to the $[010]$ direction in Ref.⁶. Experimental data from Ref.⁶ do not allow to evaluate the effect of boundary scattering, as they refer to nanowires having roughly the same size, and are smaller than all the nanowires used in Ref.⁵. Therefore, we compared the bulk thermal conductivity predictions of equation (12) with the experimental data from Ref.⁵. In the calculation of the data reported in figure (1), temperature effects are accounted through the Bose-Einstein distributions entering in the scattering operator. Accounting for the renormalization of the force constants due to temperature goes beyond the conceptual scope of this work but it has been addressed recently by several studies^{53–64}. Calculations for diamond and silicon are performed using a $26 \times 26 \times 26$ q-point grid and a smearing of 8 cm^{-1} and 4 cm^{-1} respectively. Details on the first-principles calculation of the force constants for these materials can be found in Refs.^{14,16}. In figure (2d,e), contributions to $\kappa_{C,DOS}^{xx}$ smaller than $4 \cdot 10^{-6} \frac{\text{W} \cdot \text{cm}^2}{\text{m} \cdot \text{K}}$ are

not reported for graphical clarity.

TABLE I. Lattice parameters of CsPbBr_3 in the orthorhombic phase, obtained by first-principles simulations or experiments^{6,43}. Inset: unit cell of orthorhombic CsPbBr_3 visualized with VESTA⁴²; the directions \hat{x} , \hat{y} and \hat{z} discussed e.g. in figure (1) refer respectively to lattice vectors \mathbf{a}_1 , \mathbf{a}_2 and \mathbf{a}_3 .

	a_1 [Å]	a_2 [Å]	a_3 [Å]	
Present (th)	7.963	8.389	11.632	
Ref. ⁶ (th)	7.990	8.416	11.674	
Ref. ⁴⁰ (exp)	8.198	8.244	11.735	
Ref. ⁴³ (exp)	8.223	8.243	11.761	

Data availability. Raw data were generated using the SCITAS High Performance Computing facility at the École Polytechnique Fédérale de Lausanne. Derived data supporting the findings of this study are available at <https://archive.materialscloud.org>.

Code availability. Quantum ESPRESSO is available at www.quantum-espresso.org; the scripts related to the computation of the third order force constants using the finite-difference method are available at bitbucket.org/sousaw/thirdorder; the D3Q package for Quantum ESPRESSO is available at sourceforge.net/projects/d3q/. The custom code developed in this work will be made available in a next release of the D3Q package.

-
- ¹ Peierls, R. Zur Kinetischen Theorie der Wärmeleitung in Kristallen. *Ann. Phys. (N. Y.)* **395**, 1055–1101 (1929).
- ² Allen, P. B. & Feldman, J. L. Thermal Conductivity of Glasses: Theory and Application to Amorphous Si. *Phys. Rev. Lett.* **62**, 645–648 (1989).
- ³ Sun, T. & Allen, P. B. Lattice thermal conductivity: Computations and theory of the high-temperature breakdown of the phonon-gas model. *Phys. Rev. B* **82**, 224305 (2010).
- ⁴ Li, W. & Mingo, N. Ultralow lattice thermal conductivity of the fully filled skutterudite $\text{YbFe}_4\text{Sb}_{12}$ due to the flat avoided-crossing filler modes. *Phys. Rev. B* **91**, 144304 (2015).
- ⁵ Wang, Y. *et al.* Cation Dynamics Governed Thermal Properties of Lead Halide Perovskite Nanowires. *Nano Lett.* **18**, 2772–2779 (2018).
- ⁶ Lee, W. *et al.* Ultralow thermal conductivity in all-inorganic halide perovskites. *Proc. Natl. Acad. Sci. U. S. A.* **114**, 8693–8697 (2017).
- ⁷ Chen, X. *et al.* Twisting phonons in complex crystals with quasi-one-dimensional substructures. *Nat. Commun.* **6**, 6723 (2015).
- ⁸ Voneshen, D. *et al.* Suppression of thermal conductivity by rattling modes in thermoelectric sodium cobaltate. *Nat. Mater.* **12**, 1028–1032 (2013).
- ⁹ Lory, P.-F. *et al.* Direct measurement of individual phonon lifetimes in the clathrate compound $\text{Ba}_7.81\text{Ge}_{40.67}\text{Au}_{5.33}$. *Nat. Commun.* **8**, 491 (2017).
- ¹⁰ Weathers, A. *et al.* Glass-like thermal conductivity in nanostructures of a complex anisotropic crystal. *Phys. Rev. B* **96**, 214202 (2017).
- ¹¹ Garg, J., Bonini, N., Kozinsky, B. & Marzari, N. Role of Disorder and Anharmonicity in the Thermal Conductivity of Silicon-Germanium Alloys: A First-Principles Study. *Phys. Rev. Lett.* **106**, 045901 (2011).
- ¹² Omini, M. & Sparavigna, A. An iterative approach to the phonon Boltzmann equation in the theory of thermal conductivity. *Physica B: Condens. Matter* **212**, 101 – 112 (1995).
- ¹³ Carrete, J. *et al.* almaBTE : A solver of the space-time dependent Boltzmann transport equation for phonons in structured materials. *Comput. Phys. Commun.* **220**, 351 – 362 (2017).
- ¹⁴ Fugallo, G., Lazzeri, M., Paulatto, L. & Mauri, F. Ab initio variational approach for evaluating lattice thermal conductivity. *Phys. Rev. B* **88**, 045430 (2013).
- ¹⁵ Chaput, L. Direct Solution to the Linearized Phonon Boltzmann Equation. *Phys. Rev. Lett.* **110**, 265506 (2013).
- ¹⁶ Cepellotti, A. & Marzari, N. Thermal Transport in Crystals as a Kinetic Theory of Relaxons. *Phys. Rev. X* **6**, 041013 (2016).
- ¹⁷ Cepellotti, A. *et al.* Phonon hydrodynamics in two-dimensional materials. *Nat. Commun.* **6**, 6400 (2015).
- ¹⁸ Hardy, R. J. Energy-Flux Operator for a Lattice. *Phys. Rev.* **132**, 168–177 (1963).
- ¹⁹ Allen, P. B., Feldman, J. L., Fabian, J. & Wooten, F. Diffusions, locons and propagons: Character of atomic vibrations in amorphous Si. *Philos. Mag. B* **79**, 1715–1731 (1999).

- ²⁰ Lv, W. & Henry, A. Non-negligible contributions to thermal conductivity from localized modes in amorphous silicon dioxide. *Scientific reports* **6**, 35720 (2016).
- ²¹ Ziman, J. M. *Electrons and phonons: the theory of transport phenomena in solids* (Oxford university press, 1960).
- ²² Tamura, S.-i. Isotope scattering of dispersive phonons in Ge. *Phys. Rev. B* **27**, 858–866 (1983).
- ²³ Gebauer, R. & Car, R. Kinetic theory of quantum transport at the nanoscale. *Phys. Rev. B* **70**, 125324 (2004).
- ²⁴ Frensky, W. R. Boundary conditions for open quantum systems driven far from equilibrium. *Rev. Mod. Phys.* **62**, 745–791 (1990).
- ²⁵ Cohen-Tannoudji, C., Dupont-Roc, J., Grynberg, G. & Thickstun, P. *Atom-photon interactions: basic processes and applications* (Wiley Online Library, 2004).
- ²⁶ Cahill, D. G., Watson, S. K. & Pohl, R. O. Lower limit to the thermal conductivity of disordered crystals. *Phys. Rev. B* **46**, 6131–6140 (1992).
- ²⁷ Agne, M. T., Hanus, R. & Snyder, G. J. Minimum thermal conductivity in the context of diffuson-mediated thermal transport. *Energy Environ. Sci.* **11**, 609–616 (2018).
- ²⁸ Clarke, D. R. Materials selection guidelines for low thermal conductivity thermal barrier coatings. *Surface and Coatings Technology* **163-164**, 67–74 (2003).
- ²⁹ Marcolongo, A., Umari, P. & Baroni, S. Microscopic theory and quantum simulation of atomic heat transport. *Nat. Phys.* **12**, 80 (2016).
- ³⁰ Seyf, H. R. *et al.* Rethinking phonons: The issue of disorder. *npj Comp. Mat.* **3**, 49 (2017).
- ³¹ Carbogno, C., Ramprasad, R. & Scheffler, M. Ab Initio Green-Kubo Approach for the Thermal Conductivity of Solids. *Phys. Rev. Lett.* **118**, 175901 (2017).
- ³² Puligheddu, M., Gygi, F. & Galli, G. First-principles simulations of heat transport. *Phys. Rev. Materials* **1**, 060802 (2017).
- ³³ Kané, G., Lazzeri, M. & Mauri, F. Zener tunneling in the electrical transport of quasimetallic carbon nanotubes. *Phys. Rev. B* **86**, 155433 (2012).
- ³⁴ Simoncelli, M., Marzari, N. & Mauri, F. *In preparation*.
- ³⁵ Marzari, N., Mostofi, A. A., Yates, J. R., Souza, I. & Vanderbilt, D. Maximally localized Wannier functions: Theory and applications. *Rev. Mod. Phys.* **84**, 1419–1475 (2012).
- ³⁶ Hardy, R. J. Phonon Boltzmann equation and second sound in solids. *Phys. Rev. B* **2**, 1193 (1970).
- ³⁷ Allen, P. B. & Feldman, J. L. Thermal conductivity of disordered harmonic solids. *Phys. Rev. B* **48**, 12581–12588 (1993).
- ³⁸ Auerbach, A. & Allen, P. B. Universal high-temperature saturation in phonon and electron transport. *Phys. Rev. B* **29**, 2884–2890 (1984).
- ³⁹ Feldman, J. L., Kluge, M. D., Allen, P. B. & Wooten, F. Thermal conductivity and localization in glasses: Numerical study of a model of amorphous silicon. *Phys. Rev. B* **48**, 12589–12602 (1993).
- ⁴⁰ Stoumpos, Constantinos C. and Malliakas, Christos D. and Peters, John A. and Zhifu Liu and Maria Sebastian and Jino Im and Chasapis, Thomas C. and Wibowo, Arief C. and Chung, Duck Young and Freeman, Arthur J and Wesels, Bruce W. and Kanatzidis, Mercouri G. Crystal growth of the perovskite semiconductor CsPbBr₃: A new material for high-energy radiation detection. *Cryst. Growth Des.* **13**, 2722–2727 (2013).
- ⁴¹ Gražulis, S. *et al.* Crystallography Open Database – an open-access collection of crystal structures. *J. Appl. Crystallogr.* **42**, 726–729 (2009).
- ⁴² Momma, K. & Izumi, F. VESTA 3 for three-dimensional visualization of crystal, volumetric and morphology data. *J. Appl. Crystallogr.* **44**, 1272–1276 (2011).
- ⁴³ Miyata, K. *et al.* Large polarons in lead halide perovskites. *Sci. Adv.* **3** (2017).
- ⁴⁴ Giannozzi, P. *et al.* Advanced capabilities for materials modelling with Quantum ESPRESSO. *J. Phys. Condens. Matter* **29**, 465901 (2017).
- ⁴⁵ Garrity, K. F., Bennett, J. W., Rabe, K. M. & Vanderbilt, D. Pseudopotentials for high-throughput DFT calculations. *Comput. Mater. Sci.* **81**, 446 – 452 (2014).
- ⁴⁶ Baroni, S., de Gironcoli, S., Dal Corso, A. & Giannozzi, P. Phonons and related crystal properties from density-functional perturbation theory. *Rev. Mod. Phys.* **73**, 515–562 (2001).
- ⁴⁷ Li, W., Carrete, J., Katcho, N. A. & Mingo, N. ShengBTE: A solver of the Boltzmann transport equation for phonons. *Comput. Phys. Commun.* **185**, 1747 – 1758 (2014).
- ⁴⁸ Paulatto, L., Errea, I., Calandra, M. & Mauri, F. First-principles calculations of phonon frequencies, lifetimes, and spectral functions from weak to strong anharmonicity: The example of palladium hydrides. *Phys. Rev. B* **91**, 054304 (2015).
- ⁴⁹ Togo, A., Chaput, L. & Tanaka, I. Distributions of phonon lifetimes in Brillouin zones. *Phys. Rev. B* **91**, 094306 (2015).
- ⁵⁰ Paulatto, L., Mauri, F. & Lazzeri, M. Anharmonic properties from a generalized third-order ab initio approach: Theory and applications to graphite and graphene. *Phys. Rev. B* **87**, 214303 (2013).
- ⁵¹ Chernatynskiy, A. & Phillpot, S. R. Phonon Transport Simulator (PhonTS). *Comput. Phys. Commun.* **192**, 196–204 (2015).
- ⁵² Tadano, T., Gohda, Y. & Tsuneyuki, S. Anharmonic force constants extracted from first-principles molecular dynamics: applications to heat transfer simulations. *J. Phys. Condens. Matter* **26**, 225402 (2014).
- ⁵³ Bianco, R., Errea, I., Paulatto, L., Calandra, M. & Mauri, F. Second-order structural phase transitions, free energy curvature, and temperature-dependent anharmonic phonons in the self-consistent harmonic approximation: Theory and stochastic implementation. *Phys. Rev. B* **96**, 014111 (2017).
- ⁵⁴ Tadano, T. & Tsuneyuki, S. Quartic Anharmonicity of Rattlers and Its Effect on Lattice Thermal Conductivity of Clathrates from First Principles. *Phys. Rev. Lett.* **120**, 105901 (2018).
- ⁵⁵ van Roekeghem, A., Carrete, J. & Mingo, N. Anomalous thermal conductivity and suppression of negative thermal expansion in ScF₃. *Phys. Rev. B* **94**, 020303 (2016).
- ⁵⁶ Yang, F. C. *et al.* Temperature dependence of phonons in Pd₃Fe through the Curie temperature. *Phys. Rev. B* **98**, 024301 (2018).
- ⁵⁷ Zhang, D.-B., Sun, T. & Wentzcovitch, R. M. Phonon Quasiparticles and Anharmonic Free Energy in Complex Systems. *Phys. Rev. Lett.* **112**, 058501 (2014).
- ⁵⁸ Ravichandran, N. K. & Broido, D. Unified first-principles theory of thermal properties of insulators. *Phys. Rev. B* **98**, 085205 (2018).
- ⁵⁹ Romero, A. H., Gross, E. K. U., Verstraete, M. J. & Hellman, O. Thermal conductivity in PbTe from first principles. *Phys. Rev. B* **91**, 214310 (2015).
- ⁶⁰ Aseginolaza, U. *et al.* Phonon Collapse and Second-Order Phase Transition in Thermoelectric SnSe. *arXiv preprint arXiv:1807.07726* (2018).
- ⁶¹ Hellman, O., Abrikosov, I. A. & Simak, S. I. Lattice dynamics of anharmonic solids from first principles. *Phys. Rev. B* **84**, 180301 (2011).

- ⁶² Hellman, O. & Abrikosov, I. A. Temperature-dependent effective third-order interatomic force constants from first principles. *Phys. Rev. B* **88**, 144301 (2013).
- ⁶³ Hellman, O., Steneteg, P., Abrikosov, I. A. & Simak, S. I. Temperature dependent effective potential method for accurate free energy calculations of solids. *Phys. Rev. B* **87**, 104111 (2013).
- ⁶⁴ Souvatzis, P., Eriksson, O., Katsnelson, M. I. & Rudin, S. P. Entropy Driven Stabilization of Energetically Unstable Crystal Structures Explained from First Principles Theory. *Phys. Rev. Lett.* **100**, 095901 (2008).